4-2018

Isotope Shifts in the 7 s → 8 s Transition of Francium: Measurements and Comparison to ab initio Theory

M. R. Kalita

J. A. Behr

...

Seth Aubin
William & Mary, saaubi@wm.edu

et al.

Recommended Citation

Kalita, M. R.; Behr, J. A.; ...; Aubin, Seth; and al., et, Isotope Shifts in the 7 s → 8 s Transition of Francium: Measurements and Comparison to ab initio Theory (2018). *Physical Review A*, 97(4). https://doi.org/10.1103/PhysRevA.97.042507

Isotope shifts in the $7s \rightarrow 8s$ transition of francium: Measurements and comparison to *ab initio* theory

M. R. Kalita,* J. A. Behr, A. Gorelov, and M. R. Pearson
TRIUMF, Vancouver, British Columbia, Canada, V6T 2A3

A. C. DeHart, G. Gwinner, and M. J. Kossin
Department of Physics and Astronomy, University of Manitoba, Winnipeg, Manitoba, Canada, R3T 2N2

L. A. Orozco
JQI, Department of Physics and NIST, University of Maryland, College Park, Maryland 20742, USA

S. Aubin
Department of Physics, College of William and Mary, Williamsburg, Virginia 23186, USA

E. Gomez
Instituto de Física, Universidad Autónoma de San Luis Potosí, San Luis Potosi 78290, Mexico

M. S. Safronova
Department of Physics and Astronomy, U. Delaware, Newark, Delaware 19716, USA
and JQI, Department of Physics and NIST, University of Maryland, College Park, Maryland 20742, USA

V. A. Dzuba and V. V. Flambaum
School of Physics, University of New South Wales, Sydney 2052, Australia

(Received 19 October 2017; revised manuscript received 27 March 2018; published 30 April 2018)

We observe the electric-dipole forbidden $7s \rightarrow 8s$ transition in the francium isotopes $^{208-211}$Fr and ^{213}Fr using a two-photon excitation scheme. We collect the atoms online from an accelerator and confine them in a magneto-optical trap for the measurements. In combination with previous measurements of the $7s \rightarrow 7p_{1/2}$ transition we perform a King plot analysis. We compare the thus-determined ratio of the field shift constants (1.228 ± 0.019) to results obtained from new *ab initio* calculations (1.234 ± 0.010).

DOI: 10.1103/PhysRevA.97.042507

I. INTRODUCTION

The isotope shift in the transition energies of an atom arises due to a combination of nuclear and atomic effects. It is an important benchmark, as it can provide information about the nuclear charge distribution and its change as more neutrons are added; the shift also depends on electron correlations. The FrPNC collaboration at TRIUMF has been studying francium with the ultimate goal of measuring atomic parity nonconservation (APNC) [1,2]. Others have also proposed to use francium for APNC studies [3], and to search for time-reversal violation through the existence of permanent electric dipole moment (EDM) of the electron [4,5]. These proposals require quantitative understanding of the atomic and nuclear structure, and in particular the overlap of the electronic wave functions with the nucleus. This overlap can be tested by comparing the measurements of hyperfine structure and isotope shift in chains of isotopes to the *ab initio* calculations [6].

Testing the accuracy of the *ab initio* theory for field shifts in heavy atoms is also crucial for extraction of the change of nuclear radii in superheavy elements [7] as well as for francium nuclei [8,9]. Combining theoretical and experimental isotope shift values allows the extraction of the differences in the nuclear radii of the these atoms and provides an insight into their nuclear structure. Studies of isotope shift of superheavy elements are also of interest for astrophysics [10]. All of these projects require reliable benchmarks of theoretical calculations to verify the theory uncertainties. Measurements of the field shift ratios for different atomic transitions are of particular interest owing to the recently found disagreement of the Ca^+ $D1/D2$ field shift measurement with all theoretical predictions [11]. Isotope shift measurements have also been proposed as a new method to probe new light force-mediators [12].

Here we report the observation of the electric dipole forbidden $7s \rightarrow 8s$ atomic transition in the francium isotopes $^{208-211}$Fr and ^{213}Fr using a single-frequency two-photon excitation scheme, its isotope shift and the comparison to *ab initio* theory. This transition in francium is of particular interest for APNC experiments, as it is electric-dipole forbidden by electromagnetism but slightly allowed by the weak interaction. The landmark APNC experiments in cesium performed in Paris and Boulder used the equivalent $6s \rightarrow 7s$

*Corresponding author: mkalita@triumf.ca

transition in cesium [13–15]. Our isotope shift measurements are complementary to hyperfine splitting measurements, which also depend on the wave functions at the nucleus; together with the information obtained from the change in the nuclear magnetization from the measurements of hyperfine anomalies, this allows to create a better picture of the nuclear structure [16,17]. In contrast, measurements of the electronic dipole matrix elements (obtained from lifetime measurements of excited atomic states) probe the wave functions predominantly at large distances from the nucleus [18].

We divide this paper into the following sections: In Sec. II we briefly discuss the general theory relevant for the measured isotope shifts, in Sec. III we present the theoretical calculations of the field shift, in Sec. IV we describe the experimental details, in Sec. V we discuss our experimental results, Sec. VI contains a King plot analysis and the comparison to the theoretical predictions, closing with conclusions in Sec. VII.

II. ISOTOPE SHIFTS

Single-photon electronic transitions between states of the same parity in atoms are forbidden by electric-dipole selection rules; however, a two-photon transition is allowed between states of the same parity. The selection rules for a two-photon transition where both photons are far off resonance from any intermediate states are $\Delta F = 0$ and $\Delta m_F = 0$ [19].

Using two-photon spectroscopy in our setup and previously measured hyperfine splittings of the $7s$ and $8s$ states we obtain the center of gravity (C.O.G) of the $7s \rightarrow 8s$ transition in five different isotopes of francium that we collect online from an accelerator and capture in a magneto-optical trap (MOT). From these measurements we deduce the isotope shifts and perform a King plot analysis [20]. Optical isotope shifts are discussed in detail in Refs. [6,21,22]. Here we briefly review the theory that is relevant to the measurements reported in this paper.

For heavy elements the optical isotope shift $\delta\nu_{IS}^{AA'}$, between isotopes with mass number A and A' and nuclear mass M_A and $M_{A'}$, respectively, can be written as[1]

$$\delta\nu_{IS}^{AA'} = (N + \mathcal{S})\frac{M_A - M_{A'}}{M_A M_{A'}} + F\delta\langle r^2\rangle^{AA'}. \tag{1}$$

N is the normal mass shift (NMS) constant, and $\mathcal{S}$ is the specific mass shift (SMS) constant that stems from the changing mass of the nucleus between isotopes. The contribution of the normal mass shift to the frequency of an optical transition can be written in the nonrelativistic limit as

$$\delta\nu_{\mathrm{NMS}}^{AA'} = \nu(A')\frac{m_e(M_A - M_{A'})}{M_{A'}M_A}, \tag{2}$$

where m_e is the mass of the electron and $\nu(A')$ is the transition frequency of an isotope with mass number A'.

The specific mass shift is hard to calculate accurately owing to poor convergence of the perturbation theory for this quantity. This issue has been discussed in detail in Ref. [23]. However, the contribution of the mass shift (both normal and specific) is small for heavy atoms and simple estimations should be sufficient. Moreover, an earlier study of francium isotope shifts has demonstrated that NMS and SMS strongly cancel each other and the residual is at the level of the accuracy of the theoretical field shift calculations [23].

In the traditional approach, F is the field shift constant that takes into account the modification of the Coulomb potential of a point-charge by that of the finite size of a nucleus. However, F also depends on the nuclear radius [24], and this dependence may be large for heavy atoms. Nevertheless, if we consider neighboring isotopes with small differences between mass numbers, the dependence of F on the nuclear radius between these isotopes can be neglected. We check this for the francium isotopes considered in this work.

F is a relatively simple single-electron scalar operator. Unlike $\mathcal{S}$, which is a two-electron operator of rank one, the field shift can be more easily included into the available, accurate, *ab initio* atomic methods. In this work, we use two completely different theory methods that we describe in Sec. III and compare the results for the field shift values to evaluate the theory uncertainty.

The values of the quantities N, $\mathcal{S}$, and F as defined are specific to a particular electronic transition in an atom. In our experiment, we obtain the total isotope shift $\delta\nu_{IS}^{AA'}$ for the $7s \rightarrow 8s$ transition as expressed by Eq. (1).

III. THEORETICAL CALCULATIONS OF THE FIELD SHIFTS

A. All-order method

We use a linearized variant of the relativistic coupled-cluster method with single, double, and partial triple excitations [23], which is referred to as the all-order method. The exact many-body wave function in the coupled-cluster method is represented in the form [25]

$$|\Psi\rangle = \exp(S)|\Psi^{(0)}\rangle, \tag{3}$$

where $|\Psi^{(0)}\rangle$ is the lowest-order atomic state vector. The operator S for an N electron atom consists of "cluster" contributions from one-electron, two-electron, and so on, N electron excitations of the lowest-order state vector $|\Psi^{(0)}\rangle$. Expanding the exponential in Eq. (3) in terms of the n-body excitations S_n, and limiting the expansion to terms linear in single, double, and valence triple contribution, we get the wave function of a monovalent atom in state v:

$$|\Psi_v\rangle = \{1 + S_1 + S_2 + S_{3v}\}\left|\Psi_v^{(0)}\right\rangle \tag{4}$$

$$= \Bigg[1 + \sum_{ma}\rho_{ma}a_m^\dagger a_a + \frac{1}{2}\sum_{mnab}\rho_{mnab}a_m^\dagger a_n^\dagger a_b a_a + \sum_{m\neq v}\rho_{mv}a_m^\dagger a_v + \sum_{mna}\rho_{mnva}a_m^\dagger a_n^\dagger a_a a_v + \frac{1}{6}\sum_{mnrab}\rho_{mnrvab}a_m^\dagger a_n^\dagger a_r^\dagger a_b a_a a_v\Bigg]\left|\Psi_v^{(0)}\right\rangle, \tag{5}$$

where $|\Psi_v^{(0)}\rangle$ is the lowest-order atomic state vector. In Eq. (5), $a_i^\dagger$ and a_i are the creation and annihilation operators for an electron state i, the indices m and n range over all possible

[1] In the relativistic case, $F\delta\langle r^2\rangle$ is replaced by $\tilde{F}\delta\langle r^{2\gamma}\rangle$, where $\gamma = (1 - Z^2\alpha^2)^{1/2}$ [10].

virtual states, while indices a and b range over all occupied core states. The quantities ρ are excitation coefficients. The single double (SD) method is the linearized coupled-cluster method restricted to single and double excitations only. The all-order singles-doubles-partial triples (SDpT) method is an extension of the SD method in which the dominant part of S_{3v} is treated perturbatively. A detailed description of the SDpT method is given in Ref. [23].

To derive equations for the excitation coefficients, the wave function $|\Psi_v\rangle$ is substituted into the many-body Schrödinger equation $H|\Psi_v\rangle = E|\Psi_v\rangle$, and terms on the left- and right-hand sides are matched, based on the number and type of operators they contain, giving the equations for the excitation coefficients. The Dirac-Hartree-Fock (DHF) starting potential with the inclusion of the Breit interaction is used to produce a finite basis set of the orbitals for all subsequent calculations. The equations for the excitation coefficients are solved iteratively until the valence correlation energy converges to a specified numerical accuracy. This procedure effectively sums the series of the dominant many-body perturbation theory (MBPT) terms, with each iteration picking up a new order of MBPT. Thus, the method includes dominant correlation corrections to all orders of MBPT.

B. Field-shift calculations: Method I

If we describe the nucleus as a uniformly charged ball of radius R, the change in the nuclear potential induced by a change in the nuclear radius δR, is given by

$$\delta V(r) = \frac{3Z}{2R^2}\left[1 - \frac{r^2}{R^2}\right]\delta R, \tag{6}$$

$r \leqslant R$. Rewriting this result in terms of the mean square radius $\langle r^2\rangle = (3/5)R^2$, we define a field-shift operator $F(r)$ as [26]

$$\delta V = F(r)\delta\langle r^2\rangle, \tag{7}$$

$$F(r) = \frac{5Z}{4R^3}\left[1 - \frac{r^2}{R^2}\right], \quad r \leqslant R$$
$$= 0, r > R. \tag{8}$$

When we use a more elaborate Fermi distribution to describe the nucleus

$$\rho(r) = \frac{\rho_0}{1 + \exp([r-c]/a)}, \tag{9}$$

where c is the 50% fall-off radius of the density, and a is related to the 90%–10% fall-off distance t by $t = 4\ln(3)a$, we find negligible differences with the results obtained using the formula for a simple uniform ball for the field-shift operator and a variant that uses the Fermi distribution.

In our first method we use the all-order approach and we calculate the field shift constant as an expectation value of the field-shift operator $\langle F\rangle$ given by

$$F_{wv} = \frac{\langle\Psi_w|F|\Psi_v\rangle}{\sqrt{\langle\Psi_v|\Psi_v\rangle\langle\Psi_w|\Psi_w\rangle}}, \tag{10}$$

where $|\Psi_v\rangle$ and $|\Psi_w\rangle$ are given by the expansion (5) limited to single and double excitations. The resulting expression for the numerator of Eq. (10) consists of the sum of the DHF matrix element f_{wv} and 20 other terms that are linear or quadratic functions of the excitation coefficients.

C. Field-shift calculations: Method II

In the second method, we use an all-order finite-field approach [27]. Calculations of the field shift are done for the reference isotope A with a nuclear charge radius R by replacing a nuclear potential $V(r)$ by

$$V(r) + \lambda\delta V(r), \tag{11}$$

where λ is a scaling parameter

$$\delta V(r) = \frac{dV}{dR}\delta\langle R\rangle. \tag{12}$$

The Fermi distribution is used for the charge distribution and the derivative $\frac{dV}{dR}$ is calculated numerically. The value of λ is chosen in such a way that the corresponding change in the nuclear potential is sufficiently small for the final energy to be a linear function of λ but much larger than the numerical uncertainty of the calculations. The calculations are carried out

TABLE I. Field shift constants F (in MHz/fm^2) of francium levels calculated using different methods. $\tilde{\mathcal{R}}$ is the ratio of the field shift constants for the $7s \rightarrow 7p_{1/2}$ and $7s \rightarrow 8s$ transitions defined by Eq. (14). Approximations: DHF → lowest order Dirac-Hartree-Fock, MBPT 2 → second-order many-body perturbation theory, MBPT 3 → third-order many-body perturbation theory, All-order linearized coupled-cluster method with single-double (SD) and partial triple (SDpT) excitation; SD_{sc} and $SDpT_{sc}$ are scaled results that include estimates of the dominant higher excitations. BO + fit results are obtained using the Brueckner orbitals with fitting to experimental energies.

Method	Approximation	$F(7s)$	$F(8s)$	$F(7p_{1/2})$	$F(7p_{3/2})$	$\tilde{\mathcal{R}}$
I	DHF	−14239	−3649	−485	0	1.299
I	All-order SD	−22522	−4677	−683	348	1.224
I	All-order SDpT	−21268	−4554	−674	304	1.232
I	All-order SD_{sc}	−21647	−4602	−670	333	1.231
I	All-order $SDpT_{sc}$	−21618	−4603	−687	312	1.230
II	MBPT 2	−22480	−4732	−695	311	1.227
II	MBPT 3	−19441	−4359	−455	449	1.259
II	BO+fit	−20947	−4381	−670	310	1.224
II	All-order SD	−21236	−4436	−675	333	1.224
II	All-order SD+E3	−20181	−4322	−599	371	1.235
II	All-order SDpT	−20582	−4421	−635	338	1.234
II	Final	−20580(650)	−4420(100)	−635(40)	338(33)	1.234(10)

for several values of λ and the field shift constant for an atomic state v is calculated as a derivative

$$F = \frac{dE_v(\lambda)}{d\lambda}. \quad (13)$$

Therefore, the calculation of the field shift constants reduces to the calculation of the energy in this method.

D. Theory results and discussion

The results for the field-shift constants F of francium levels calculated using both methods are given in Table I. $\tilde{\mathcal{R}}$ is the ratio of the field shift constants for the $7s \rightarrow 7p_{1/2}$ and $7s \rightarrow 8s$ transitions

$$\tilde{\mathcal{R}} = \frac{F(7p_{1/2}) - F(7s)}{F(8s) - F(7s)}. \quad (14)$$

Results obtained in several approximations are given for both methods. The DHF lowest order matrix elements are given to show the size of the correlation corrections. The all-order single-double (SD) and partial triple (SDpT) results are listed in the SD and SDpT rows. In method I, some classes of omitted contributions from higher excitations may be estimated by the scaling procedure described in Ref. [23], these results are listed with the subscript "sc." For method II, we also include the field shift constants obtained using the second- and third-order MBPT energy calculations to show the size of the third- and higher-order corrections. The energy in the SD approximation is missing a part of the third-order contribution, which is restored in the results in the "SD + E3" row. The SDpT energies include a complete third-order contribution and do not need to be corrected. We also carried out other calculation using Brueckner orbitals (BO) with fitting of the correlation potential to the experimental energies, described in Ref. [27]. The results are listed in the row labeled "BO + fit". We take the *ab initio* method II SDpT results as final. This method (method II) includes correlation corrections in a more complete way than method I. For example, applying method II already in the lowest order includes correlation correction terms, which correspond to the random-phase-approximation (RPA) in method I. We verified that both methods give the same results at the RPA level. The uncertainties are estimated from the spread of the all-order results (the methods to determine the theoretical uncertainties in the framework of the all-order approach have been extensively tested on a variety of systems and atomic quantities as discussed in Refs. [23,28,29]). We note that the uncertainty of the $7s$ field shift constant was underestimated in Ref. [27]. The relative uncertainty in the ratio $\tilde{\mathcal{R}}$ is smaller than the uncertainties in the field-shift constants for each level as correlation corrections to the $7s$ and $8s$ states are similar, and the field shift for the $7p_{1/2}$ level is small in comparison to the field shifts of the $7s$ and $8s$ levels.

IV. EXPERIMENTAL SETUP

We use francium ions produced at the Isotope Separator and Accelerator (ISAC) facility at TRIUMF. The ions are delivered to our experiment at the rate of 4×10^7/s to 2×10^9/s, and we collect them online on a zirconium foil neutralizer of area 19×12 mm^2 and of thickness 0.03 mm. Typically, we collect the ions on the foil for 20 s before rotating the foil by 90° and electrically heating it for 1 s to release neutral francium atoms from the heated foil (with maximum efficiency of 30%). We collect the released atoms first in a MOT inside a coated glass cell (collection chamber), then we transfer the atoms to another MOT inside a stainless steel vacuum chamber (science chamber, with maximum transfer efficiency of 20% for this work), by pushing them with a pulse of laser light resonant with the $D2$ line in francium at 718 nm [30]. The MOT in the science chamber is located at 0.7 m, directly below the MOT in the collection chamber. We operate both MOTs on the $D2$ line of francium and they share two Ti:Sapphire lasers. We use one laser (MSquared SolsTIS) for trapping, and we use the other laser (Coherent 899-21) for repumping the atoms. We maintain a pressure of $\approx 2 \times 10^{-10}$ Torr in the science chamber. A detailed description of the francium trapping facility (FTF) can be found in Refs. [30,31]. We can operate our apparatus with a range of isotopes ($^{206-213,221}$Fr) by adjusting our trap and repump laser frequencies, and requesting a specific isotope from ISAC [32].

We perform two-photon spectroscopy using atoms confined in the MOT in the science chamber. We use a third Ti:Sapphire laser (MSquared SolsTIS) at 1012 nm as our spectroscopy laser to excite the $7s(F = U) \rightarrow 8s(F = U)$ transition, where $F = U(L)$ is the upper(lower) hyperfine level of the s states (Fig. 2).

We lock the frequencies of all three lasers to a stabilized HeNe laser (Melles-Griot 05-STP-901) using a computer-controlled feedback system [33].

The linearly polarized spectroscopy laser beam of 350 mW power is focused to $1/e^2$ (intensity) diameter of 0.015 cm, using an achromatic lens of 30-cm focal length. The lens is mounted on a translational stage to fine-tune the overlap of the laser beam with the atom cloud. To increase the average intensity of the spectroscopy beam across the atom cloud, the beam is recollimated and refocused back on itself in a double-pass scheme using a second 30-cm focal length lens and a mirror. An optical isolator (LINOS, FI-980-TI) is necessary to reduce optical feedback into the laser.

We apply a frequency offset between the beam pick off for locking and the spectroscopy laser beam directed at the atom cloud by using an acousto-optic modulator (AOM) in double-pass configuration as shown in Fig. 1. We ramp the RF offset by 18.86 MHz over 12 s [a 37.72 MHz scan across the $7s(F = U) \rightarrow 8s(F = U)$ resonance]. To maintain the lock, the feedback system shifts the laser and hence the spectroscopy beam in frequency.

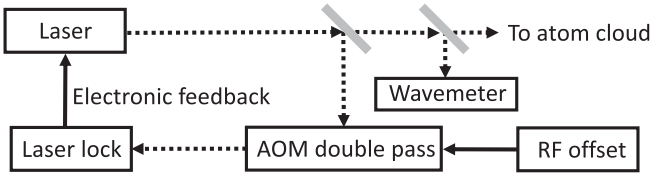

FIG. 1. Simplified schematic showing the setup for scanning the spectroscopy laser. Dotted and solid arrows depict optical and electronic signals, respectively. To scan the laser frequency we ramp the RF offset.

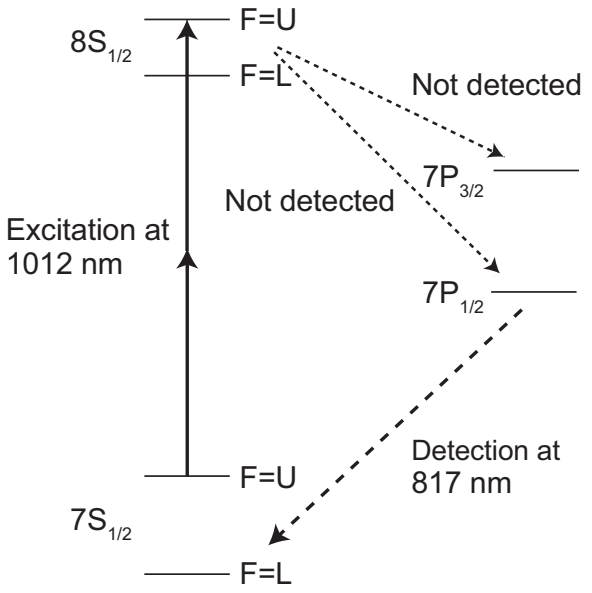

FIG. 2. Energy level diagram for francium with relevant transitions. Atoms in the $7s$ state are excited to the $8s$ state with two 1012-nm spectroscopy laser photons (solid arrows). The spontaneous decay (dashed arrows) via the $7p_{1/2}$ level is detected at 817 nm. This figure is not to scale.

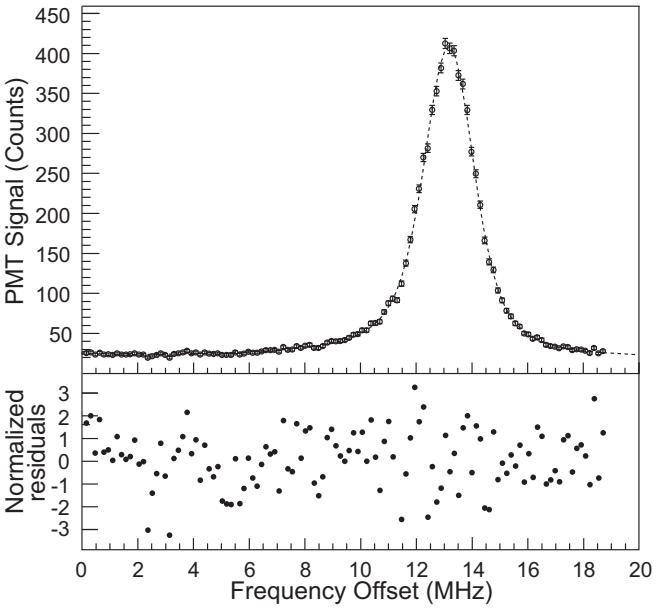

FIG. 3. Two-photon spectroscopy data for the $7s(F = 5) \rightarrow 8s(F = 5)$ transition in ^{211}Fr. The vertical axis shows PMT counts of 817-nm photons. The frequency scan starts at the zero of the horizontal axis. The dashed line is a fit to the data (see text). The bottom plot shows the normalized residuals of the fit.

We detect the resonance of the $7s(F = U) \rightarrow 8s(F = U)$ transition by collecting 817-nm photons resulting from the decay of atoms from the $7p_{1/2}$ state to the $7s$ ground state ($D1$ line of francium and about 100 nm away from the $D2$ line as shown in Fig. 2).

We direct the 817-nm photons onto a photomultiplier tube (PMT, Hamamatsu H7422 operated in photon counting mode) using a double-relay optical system. To reduce background counts from the trap beams at 718 nm, we place an edge filter (Semrock LP02-785RU) and a longpass colored glass filter (Thorlabs FGL780M) in front of the PMT. The 718-nm light scattered by the MOT does not contribute significantly to our background counts. We save PMT data as a function of time for later analysis. The beginning of the offset frequency scan and the beginning of PMT data collection is synchronized using a digital trigger. During the scans, the trap light is cycled on and off with a 2-ms period (50% duty cycle) and with an extinction ratio of 1000:1, while the repumper and spectroscopy light remain on continuously. We collect data when the trap light is off to suppress the ac Stark shift that it produces, as well as to minimize background counts. During each MOT collection-transfer cycle, we perform a single offset frequency scan of the spectroscopy laser.

V. EXPERIMENTAL RESULTS

The hyperfine interaction splits the s states into two hyperfine levels. We measure transition frequencies from the upper hyperfine level of the $7s$ ground state to the upper hyperfine level of the $8s$ excited state (Fig. 2) in five different isotopes of francium: ^{208}Fr (radioactive half-life $T_{1/2} = 59$ s), ^{209}Fr (50 s), ^{210}Fr (192 s), ^{211}Fr (186 s), and ^{213}Fr (35 s). Figure 3 shows typical 817-nm fluorescence for the scan of the two photon excitation in the isotope ^{211}Fr. Ten scans of 12-s duration each are used to generate this plot. The separation between bins is 157 kHz.

To determine the center frequency of the fluorescence peak, we fit the data to a Voigt function (V) and an exponentially decaying function using the ROOT package,

$$y = a_0 + a_1 e^{-x/a_2} V(a_3; a_4, a_5). \tag{15}$$

The exponential decay takes into account the rate of loss of atoms from the trap (the $1/e$ lifetime of the atoms in the trap can be as long as 14 ± 3 s) during the laser scans. The program uses the 'MINUIT" function minimization routines to find the best parameters that minimize the χ^2 of the fit [34]. We float the following fit parameters: background level (a_0), peak height (a_1), $1/e$ decay constant (a_2), peak position (a_3), and width [Gaussian(a_4) and Lorentzian(a_5)]. Over the five isotopes, the χ^2/(degree of freedom) for the fits varies from 1.2 to 1.8. To check that the distribution of normalized residuals of each fit is consistent with a Gaussian of mean $\mu = 0$ and variance $\sigma^2 = 1$, we perform the Kolmogorov-Smirnov test. The P values of the tests range from 0.8 to 0.08.

The $7s(F = U) \rightarrow 8s(F = U)$ transition energy ν_0 is given by the relation $\nu_0 = 2 \times (\nu_f + \nu_w)$, where ν_f is the offset frequency of the peak determined from the fit and ν_w is the probe laser frequency at the beginning of a scan, which we measure using a wavemeter (Angstrom WS-U-10) as shown in Fig .1. The multiplying factor of 2 is due to two-photon nature of the transition that we excite.

While the absolute frequency accuracy of the wavemeter is only about 20 MHz, it provides over several hours a precision (reproducibility) of 1 MHz or better within a band of several GHz at 1012 nm, covering the isotopes under investigation. In

addition, we estimate the jitter of the cavity lock and feedback system to the laser to contribute about 1 MHz uncertainty to the frequency scale of the scan. The 1σ errors in peak positions for the different isotopes obtained from the fitting program are found to be in the range from 10 kHz to 63 kHz, which contributes little to the overall uncertainty in determining ν_0.

The ac Stark shift due to the trap light at 718 nm is reduced by extinguishing the trap light by a factor of 1000 during data collection yielding a negligible contribution to the uncertainty.

The ac Stark shift of the 1012-nm light that we use to drive the $7s \rightarrow 8s$ transition was theoretically studied in Refs. [35,36]. For our typical 1012-nm laser power of 350 mW and beam diameter of 150 μm, the estimated shift is < 50 kHz. The laser power is typically stable at the $< 5\%$ level, and the error on our measurements due to this effect is negligible.

The energy levels involved in the $7s(F = U) \rightarrow 8s(F = U)$ transition have similar g factors and hence similar Zeeman effects. There is no linear shift in the measured transition frequency due to the magnetic field gradient of 10 G/cm of our MOT (this is due to the $\Delta m_F = 0$ selection rule). The cold atom cloud has a diameter of about 1 mm and resides close to the zero of the magnetic field. We do not include any error or systematic shift on the isotope shift measurements due to magnetic fields.

Overall, these considerations allow us to determine the frequency ν_0 with 2.8 MHz uncertainty up to an unknown constant offset of order 20 MHz common to all isotopes and hence canceling out of our isotope shift measurements.

To determine the isotope shifts we need to calculate the center of gravity (C.O.G) of the $7s \rightarrow 8s$ transition. To do this, we use our measurement of ν_0 in the five isotopes together with previously published measurements of the hyperfine splittings of the $7s$ state of the isotopes [37], and the hyperfine splittings of the $8s$ state in ^{210}Fr [38]. Considering that the ratio of the hyperfine splittings of the $7s$ and the $8s$ state are the same across the isotopes (s states have to first-order identical hyperfine anomalies), we determine the C.O.G. of the $7s \rightarrow 8s$ transition in the five isotopes. We obtain the isotope shifts of the $7s \rightarrow 8s$ transition by subtracting the C.O.G. of the transition in the isotopes from the C.O.G. of the same transition in ^{213}Fr.

We determine the error in our calculation of the C.O.G.s, by using the 2.8 MHz error of ν_0 together with the reported errors in the measurements of the hyperfine constants of the $7s$ and $8s$ states from Refs. [37,38]. From these references, we deduce the errors in the hyperfine splittings of the isotopes in the $7s$ state to be in the range from 3 to 6 MHz, while the errors in the $8s$ hyperfine splittings to be in the range from 6.5 to 7.6 MHz. The results from our measurements and the isotope shifts in the $D1$ line of francium from Refs. [32,39] are shown in Table II. The isotope shifts in the $D1$ line are calculated for this analysis from data reported in Ref. [32], using ^{213}Fr as the reference isotope. For ^{213}Fr we measure the resonance of the $7s(F = U) \rightarrow 8s(F = U)$ transition to be $2 \times 9865.95081(9)$ cm^{-1} up to a possible systematic shift of the order $\pm$ 0.00133 cm^{-1} (prior to the measurement, the wavemeter was calibrated with a diode laser referenced by saturated absorption to the $5s(F = 2) \rightarrow 5p_{3/2}(F = 3)$ transition of ^{87}Rb [40]).

The measurement of these isotope shifts could be improved to provide a more stringent test of the theory. This would need, in addition to reduction of the presently listed uncertainties of the $7s(F = U) \rightarrow 8s(F = U)$ transition, remeasurements at higher accuracy the hyperfine splittings of the $7s$ and the $8s$ states. Note that selection rules forbid a direct measurement of the s state hyperfine splittings by using this two-photon transition.

TABLE II. Isotope shifts in the $7s \rightarrow 8s$ transition ($\delta\nu_{IS,SS}$) (this work), and isotopes shifts in the D1 line ($\delta\nu_{IS,D_1}$) based on measurements reported in Ref. [32]. For the errors (numbers inside parentheses) the common systematic shift does not contribute (see text).

		This work	Ref. [32]
Isotope	Nuclear spin (I)	$\delta\nu_{IS,SS}$ (MHz)	$\delta\nu_{IS,D_1}$ (MHz)
208	7	−5124(7)	−6341(5)
209	9/2	−3678(6)	−4563(4)
210	6	−3274(6)	−4058(4)
211	9/2	−1958(6)	−2431(4)
213	9/2	0	0

VI. KING PLOT ANALYSIS

To perform the King plot analysis, we plot the modified isotope shifts of the $D1$ line against the modified isotope shift of the $7s \rightarrow 8s$ transition. This gives a straight line [20] according to the relationship

$$\frac{M_A M_{A'}}{M_A - M_{A'}}\delta\nu_{IS,D1} = \frac{F_{D1}}{F_{SS}}\frac{M_A M_{A'}}{M_A - M_{A'}}\delta\nu_{IS,SS} + (N_{D1} + \mathcal{S}_{D1}) - \frac{F_{D1}}{F_{SS}}(N_{SS} + \mathcal{S}_{SS}), \tag{16}$$

where $N_{D1}(N_{SS})$, $\mathcal{S}_{D1}(\mathcal{S}_{SS})$, and $F_{D1}(F_{SS})$ are the normal mass shift, specific mass shift, and the field shift of the $D1(7s \rightarrow 8s)$ transition, with M_A the mass of the reference isotope. The resulting King plot is shown in Fig. 4. We fit the data to a straight line in ROOT using 'MINUIT" to minimize the χ^2, taking into account errors in both the horizontal and the vertical directions [42]. We find the value of χ^2/(degree of freedom) from the fit to be 0.52. This corresponds to a P value of 0.59. The slope is equal to the ratio of the field shift constants of the $D1$ transition and the $7s \rightarrow 8s$ transition according to Eq. (16). This represents the ratio of the change in electron densities at the nucleus during the corresponding transitions. Since an $8s$ electron has a larger probability density at the nucleus compared to a $7p_{1/2}$ electron, the ratio of the field shift constants is expected to be greater than 1. From the fit we find $\frac{F_{D1}}{F_{SS}} = 1.228 \pm 0.019$. We compare this result to the theoretical value of $\tilde{\mathcal{R}}$ [Eq. (14)] of 1.234 ± 0.010 from Table I and find agreement. From the intercept of the straight line, we find $(N_{D1} + \mathcal{S}_{D1}) - \frac{F_{D1}}{F_{SS}}(N_{SS} + \mathcal{S}_{SS}) = (-0.50 \pm 0.84) \times 10^6$ MHz amu. The errors reported here for the slope and the intercept are the 1σ errors obtained from the fit. The normal mass shift constants are $N_{D1} = 201$ GHz amu for the $D1$ transition and $N_{SS} = 325$ GHz amu for the $7s \rightarrow 8s$ transition. From this follows $\mathcal{S}_{D1} - \frac{F_{D1}}{F_{SS}}\mathcal{S}_{SS} = -302(840)$ GHz amu.

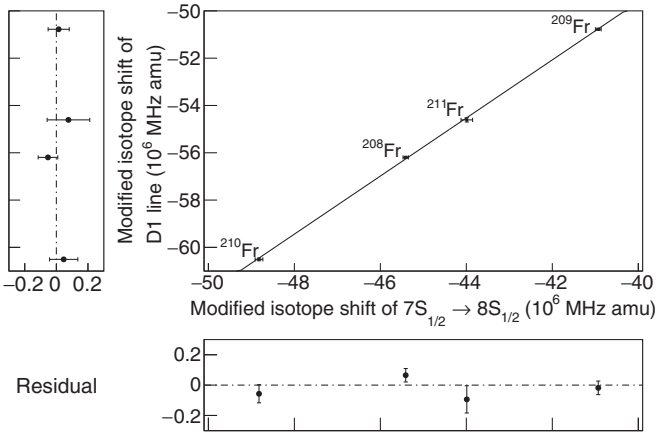

FIG. 4. The modified isotope shift of the $D1$ line is plotted against the modified isotope shift of the $7s \rightarrow 8s$ transition (following relationship 16) for the isotopes ^{208}Fr, ^{209}Fr, ^{210}Fr, and ^{211}Fr relative to ^{213}Fr. The solid line is a fit to the data. The error bars are calculated from the errors reported in Table II and the reported error in the masses of the isotopes [41].

VII. CONCLUSION

We observe the $7s \rightarrow 8s$ transition in five different isotopes of francium using a two-photon excitation scheme. We combine our measurements with previous studies of the $7s \rightarrow 7p_{1/2}$ transition and perform a King plot analysis to obtain the ratio of the field shift constants. To extract weak interaction physics from APNC data, the overlap of the relevant electron wave functions with the nucleus has to be understood. This overlap can be experimentally probed with isotope shifts and hyperfine splittings. In both cases, the extraction of the overlap is hampered by the lack of independent, precise, knowledge of the involved nuclear quantities, $\delta\langle r^2\rangle^{AA'}$ for isotope shifts, and the nuclear magnetic moment in the case of hyperfine splittings. The King plot approach is unique in its ability to reduce the influence of nuclear properties from isotope shift data, yielding a purely electronic observable, the ratio of field shift constants. It is hence a good gauge of the ability of atomic many-body calculation to describe the francium atom at a level necessary for the interpretation of future APNC measurements (see Ref. [43] for new approaches using hyperfine splittings). Our comparison to new *ab initio* theory finds agreement.

ACKNOWLEDGMENTS

We thank the ISAC staff at TRIUMF for developing the francium beam and Mikhail Kozlov for helpful discussions. The francium experiment is operated with NSERC (Canada) and NSF PHY-1307536 (USA) grants and was established with equipment funds by DOE (USA) and NSERC (Canada). TRIUMF receives federal funding through a contribution agreement with the National Research Council of Canada. M.S.S. is supported by NSF grant PHY-1620687 (USA) and the UNSW group by the Australian Research Council. M.S.S. thanks the School of Physics at UNSW, Sydney, Australia for hospitality and acknowledges support from the Gordon Godfrey Fellowship program, UNSW. S.A. acknowledges support from Fulbright Canada, and E.G. from CONACYT (Mexico). A.C.dH. and M.J.K. were supported in part via the University of Manitoba GETS program.

[1] G. Gwinner, E. Gomez, L. A. Orozco, A. Perez Galvan, D. Sheng, Y. Zhao, G. D. Sprouse, J. A. Behr, K. P. Jackson, M. R. Pearson, S. Aubin, and V. V. Flambaum, Fundamental symmetries studies with cold trapped francium atoms at ISAC, in *TCP 2006: Proceedings of the 4th International Conference on Trapped Charged Particles and Fundamental Physics (TCP 2006) held in Parksville, Canada, 3–8 September, 2006*, edited by J. Dilling, M. Comyn, J. Thompson, and G. Gwinner (Springer, Berlin, 2007), pp. 45–51.

[2] E. Gomez, S. Aubin, G. D. Sprouse, L. A. Orozco, and D. P. DeMille, Measurement method for the nuclear anapole moment of laser-trapped alkali-metal atoms, Phys. Rev. A **75**, 033418 (2007).

[3] S. N. Atutov, V. Biancalana, A. Burchianti, R. Calabrese, L. Corradi, A. Dainelli, V. Guidi, A. Khanbekyan, B. Mai, C. Marinelli, E. Mariotti, L. Moi, S. Sanguinetti, G. Stancari, L. Tomassetti, and S. Veronesi, Production and trapping of francium atoms, Nucl. Phys. A **746**, 421 (2004).

[4] B. J. Wundt, C. T. Munger, and U. D. Jentschura, Quantum Dynamics in Atomic-Fountain Experiments for Measuring the Electric Dipole Moment of the Electron with Improved Sensitivity, Phys. Rev. X **2**, 041009 (2012).

[5] T. Inoue, S. Ando, T. Aoki, H. Arikawa, S. Ezure, K. Harada, T. Hayamizu, T. Ishikawa, M. Itoh, K. Kato, H. Kawamura, A. Uchiyama, T. Aoki, K. Asahi, T. Furukawa, A. Hatakeyama, K. Hatanaka, K. Imai, T. Murakami, H. S. Nataraj, T. Sato, Y. Shimizu, T. Wakasa, H. P. Yoshida, A. Yoshimi, and Y. Sakemi, Experimental search for the electron electric dipole moment with laser cooled francium atoms, Hyperfine Interact. **231**, 157 (2015).

[6] W. H. King, *Isotope Shifts in Atomic Spectra, Physics of Atoms and Molecules* (Plenum, New York, 1984).

[7] M. Laatiaoui, W. Lauth, H. Backe, M. Block, D. Ackermann, B. Cheal, P. Chhetri, C. E. Düllmann, P. van Duppen, J. Even, R. Ferrer, F. Giacoppo, S. Götz, F. P. Heßberger, M. Huyse, O. Kaleja, J. Khuyagbaatar, P. Kunz, F. Lautenschläger, A. K. Mistry, S. Raeder, E. M. Ramirez, T. Walther, C. Wraith, and A. Yakushev, Atom-at-a-time laser resonance ionization spectroscopy of nobelium, Nature (London) **538**, 495 (2016).

[8] A. Voss, F. Buchinger, B. Cheal, J. E. Crawford, J. Dilling, M. Kortelainen, A. A. Kwiatkowski, A. Leary, C. D. P. Levy, F. Mooshammer, M. L. Ojeda, M. R. Pearson, T. J. Procter, and W. Al Tamimi, Nuclear moments and charge radii of neutron-deficient francium isotopes and isomers, Phys. Rev. C **91**, 044307 (2015).

[9] K. M. Lynch, T. E. Cocolios, J. Billowes, M. L. Bissell, I. Budinčević, T. Day Goodacre, R. P. de Groote, G. J. Farooq-Smith, V. N. Fedosseev, K. T. Flanagan, S. Franchoo, R. F. Garcia Ruiz, H. Heylen, R. Li, B. A. Marsh, G. Neyens, R. E. Rossel, S. Rothe, H. H. Stroke, K. D. A. Wendt, S. G. Wilkins, and X. Yang, Combined high-resolution laser spectroscopy and nuclear

decay spectroscopy for the study of the low-lying states in ^{206}Fr, ^{202}At, and ^{198}Bi, Phys. Rev. C **93**, 014319 (2016).

[10] V. A. Dzuba, V. V. Flambaum, and J. K. Webb, Isotope shift and search for metastable superheavy elements in astrophysical data, Phys. Rev. A **95**, 062515 (2017).

[11] C. Shi, F. Gebert, C. Gorges, S. Kaufmann, W. Nörtershäuser, B. K. Sahoo, A. Surzhykov, V. A. Yerokhin, J. C. Berengut, F. Wolf, J. C. Heip, and P. O. Schmidt, Unexpectedly large difference of the electron density at the nucleus in the $4p\,^2P_{1/2,3/2}$ fine-structure doublet of Ca^+, Appl. Phys. B **123**, 2 (2017).

[12] J. C. Berengut, D. Budker, C. Delaunay, V. V. Flambaum, C. Frugiuele, E. Fuchs, C. Grojean, R. Harnik, R. Ozeri, G. Perez, and Y. Soreq, Probing New Light Force-Mediators by Isotope Shift Spectroscopy, Phys. Rev. Lett. **120**, 091801 (2018).

[13] S. C. Bennett and C. E. Wieman, Measurement of the $6S \rightarrow 7S$ Transition Polarizability in Atomic Cesium and an Improved Test of the Standard Model, Phys. Rev. Lett. **82**, 2484 (1999).

[14] C. S. Wood, S. C. Bennett, J. L. Roberts, D. Cho, and C. E. Wieman, Precision measurement of parity nonconservation in cesium, Can. J. Phys. **77**, 7 (1999).

[15] M. A. Bouchiat, J. Guena, L. Hunter, and L. Pottier, Observation of a parity violation in cesium, Phys. Lett. B **117**, 358 (1982).

[16] J. S. Grossman, L. A. Orozco, M. R. Pearson, J. E. Simsarian, G. D. Sprouse, and W. Z. Zhao, Hyperfine Anomaly Measurements in Francium Isotopes and the Radial Distribution of Neutrons, Phys. Rev. Lett. **83**, 935 (1999).

[17] J. Zhang, M. Tandecki, R. Collister, S. Aubin, J. A. Behr, E. Gomez, G. Gwinner, L. A. Orozco, M. R. Pearson, and G. D. Sprouse (FrPNC collaboration), Hyperfine Anomalies in fr: Boundaries of the Spherical Single Particle Model, Phys. Rev. Lett. **115**, 042501 (2015).

[18] E. Gomez, L. A. Orozco, and G. D. Sprouse, Spectroscopy with trapped francium: Advances and perspectives for weak interaction studies, Rep. Prog. Phys. **69**, 79 (2006).

[19] G. Cagnac, B. Grynberg, and F. Biraben, Spectroscopie d'absorption multiphotonique sans effet Doppler, J. Phys. **34**, 845 (1973).

[20] W. H. King, Comments on the article "peculiarities of the isotope shift in the samarium spectrum", J. Opt. Soc. Am. **53**, 638 (1963).

[21] G. Fricke, C. Bernhardt, K. Heilig, L. A. Schaller, L. Schellenberg, E. B. Shera, and C. W. Dejager, Nuclear ground state charge radii from electromagnetic interactions, At. Data Nucl. Data Tables **60**, 177 (1995).

[22] I. Angeli and K. P. Marinova, Table of experimental nuclear ground state charge radii: An update, At. Data Nucl. Data Tables **99**, 69 (2013).

[23] M. S. Safronova and W. R. Johnson, All-order methods for relativistic atomic structure calculations, Adv. Atom. Mol. Opt. Phys. **55**, 191 (2008).

[24] V. V. Flambaum, A. J. Geddes, and A. V. Viatkina, Isotope shift, non-linearity of King plot and search for nuclear island of stability and new particles, Phys. Rev. A **97**, 032510 (2018).

[25] F. Coester and H. Kümmel, Short-range correlations in nuclear wave functions, Nucl. Phys. **17**, 477 (1960).

[26] W. R. Johnson, *Atomic Structure Theory: Lectures on Atomic Physics* (Springer-Verlag, Berlin, 2007).

[27] V. A. Dzuba, W. R. Johnson, and M. S. Safronova, Calculation of isotope shifts for cesium and francium, Phys. Rev. A **72**, 022503 (2005).

[28] J. Mitroy, M. S. Safronova, and C. W. Clark, Topical review: Theory and applications of atomic and ionic polarizabilities, J. Phys. B: At. Mol. Opt. Phys **43**, 202001 (2010).

[29] J. S. M. Ginges and V. V. Flambaum, Violations of fundamental symmetries in atoms and tests of unification theories of elementary particles, Phys. Rep. **397**, 63 (2004).

[30] J. Zhang, R. Collister, K. Shiells, M. Tandecki, S. Aubin, J. A. Behr, E. Gomez, A. Gorelov, G. Gwinner, L. A. Orozco, M. R. Pearson, and Y. Zhao, Efficient inter-trap transfer of cold francium atoms, Hyperfine Interact. **237**, 150 (2016).

[31] M. Tandecki, J. Zhang, R. Collister, S. Aubin, J. A. Behr, E. Gomez, G. Gwinner, L. A. Orozco, and M. R. Pearson, Commissioning of the francium trapping facility at TRIUMF, J. Instrum. **8**, P12006 (2013).

[32] R. Collister, G. Gwinner, M. Tandecki, J. A. Behr, M. R. Pearson, J. Zhang, L. A. Orozco, S. Aubin, and E. Gomez (FrPNC Collaboration), Isotope shifts in francium isotopes $^{206-213}$Fr and ^{221}Fr, Phys. Rev. A **90**, 052502 (2014).

[33] W. Z. Zhao, J. E. Simsarian, L. A. Orozco, and G. D. Sprouse, A computer-based digital feedback control of frequency drift of multiple lasers, Rev. Sci. Instrum. **69**, 3737 (1998).

[34] R. Brun and F. Rademakers, Root an object oriented data analysis framework, Nucl. Instrum. Methods Phys. Res., Sect. A **389**, 81 (1997).

[35] U. Dammalapati, K. Harada, and Y. Sakemi, Magic and tune-out wavelengths for atomic francium, Phys. Rev. A **93**, 043407 (2016).

[36] S. Singh, B. K. Sahoo, and B. Arora, Determination of magic wavelengths for the $7s^2s_{1/2} - 7p^2p_{3/2,1/2}$ transitions in fr, Phys. Rev. A **94**, 023418 (2016).

[37] A. Coc, C. Thibault, F. Touchard, H. T. Duong, P. Juncar, S. Liberman, J. Pinard, J. Lermé, J. L. Vialle, S. Büttgenbach, A. C. Mueller, and A. Pesnelle, Hyperfine structures and isotope shifts of $^{207-213,220-228}$Fr; possible evidence of octupolar deformation, Phys. Lett. B **163**, 66 (1985).

[38] J. E. Simsarian, W. Z. Zhao, L. A. Orozco, and G. D. Sprouse, Two-photon spectroscopy of the francium $8S_{1/2}$ level, Phys. Rev. A **59**, 195 (1999).

[39] R. Collister, G. Gwinner, M. Tandecki, J. A. Behr, M. R. Pearson, J. Zhang, L. A. Orozco, S. Aubin, and E. Gomez, Erratum: Isotope shifts in francium isotopes $^{206-213}$Fr and ^{221}Fr [Phys. Rev. A 90, 052502 (2014)], Phys. Rev. A **92**, 019902(E) (2015).

[40] J. Ye, S. Swartz, P. Jungner, and J. L. Hall, Hyperfine structure and absolute frequency of the ^{87}Rb $5P_{3/2}$ state, Opt. Lett. **21**, 1280 (1996).

[41] J. S. Coursey, D. J. Schwab, J. J. Tsai, and R. A. Dragoset, Atomic Weights and Isotopic Compositions (version 4.1). [Online] Available: http://physics.nist.gov/Comp [2017,04, 07] (National Institute of Standards and Technology, Gaithersburg, MD, 2015).

[42] W. H. Press, S. A. Teukolsky, W. T. Vetterling, and B. P. Flannery, *Numerical Recipes 3rd Edition: The Art of Scientific Computing*, 3rd ed. (Cambridge University Press, New York, 2007).

[43] J. S. M. Ginges and A. V. Volotka, Testing atomic wave functions in the nuclear vicinity: The hyperfine structure with empirically-deduced nuclear and quantum electrodynamic effects, arXiv:1707.00551.